RSC Advances

A theranostic polycation containing trehalose and lanthanide chelate domains for siRNA delivery and monitoring

Journal:	*RSC Advances*
Manuscript ID:	RA-COM-07-2015-014325
Article Type:	Communication
Date Submitted by the Author:	27-Jul-2015

Complete List of Authors:	Xue, Lian; University of Minnesota, Chemistry Kelkar, Sneha; Virginia Tech, Chemistry Wang, Xiaoling; Virginia Tech, Department of Chemistry and Macromolecules and Interfaces Institute Ma, Jie; University of Minnesota, Chemistry Madsen, Louis; Virginia Tech, Chemistry Reineke, Theresa; University of Minnesota, Chemistry

A theranostic polycation containing trehalose and lanthanide chelate domains for siRNA delivery and monitoring

Lian Xue[†], Sneha S. Kelkar[§,‡], Xiaoling Wang[§], Jie Ma[†], Louis A. Madsen[§] and Theresa M. Reineke[†]*.

A trehalose-based polycation that contains lanthanide-chelate domains has been examined as a theranostic vehicle for siRNA delivery. By chelating the polymers with gadolinium and terbium ions, the polymers offer magnetic resonance and luminescence-based observation properties. Lanthanide resonance energy transfer (LRET) studies were examined with the Tb^{3+}-chelated polymers (LRET donor) to monitor polyplex association with the LRET acceptor tetramethylrhodamine (TMR)-labeled siRNA. The polyplex formulations were compared to structures that do not contain trehalose within the polymer backbone and it was found that the presence of trehalose appears to increase siRNA delivery and gene knockdown efficiency in cultured glioblastoma cells (U87) that stably express luciferase. This study thus provides a preliminary theranostic polymer design model for delivery and monitoring of siRNA delivery

Theranostic nanomaterials combine features that include therapeutic delivery and diagnostic imaging. Uniting the ability to visualize pathological tissues and guide therapeutic delivery via theranostic systems show promise for aiding in personalized treatments for various diseases. These systems are of critical interest for delivery of numerous functional biological molecules that range from small molecule drugs and peptides to proteins, siRNA, and pDNA.[1]

A variety of imaging agents, including fluorescent markers[2,3], MRI contrast agents[4,5,6], and radio-labeled carriers[7] have been examined to monitor biological delivery processes. Previously, we have created polycationic delivery vehicles containing gadolinium (Gd^{3+}), terbium (Tb^{3+}), or europium (Eu^{3+}) chelates that have been shown to successfully deliver pDNA to HeLa cells and enable polyplex imaging via fluorescence microscopy and MRI.[5,6,8,9] In addition, FRET (Förster resonance energy transfer), which indicates non-radiative energy transfer between two chromophores in a distance dependent manner, has been applied to examine a variety of biomaterials.[10,11,12,13,14] For example, release of pDNA from polyplexes (polymer-pDNA complexes) has been monitored by functionalizing delivery systems and the nucleic acids with Cy3 and Cy5, which are FRET pairs.[10] FRET systems have also been reported for monitoring siRNA delivery and release.[10,15] Endres et. al. have developed core-shell nanostructures containing PEG-PCL-PEI [poly(ethylene glycol)-poly(ε-caprolactone)-poly(ethyleneimine)] triblock copolymers loaded with quantum dots, and the complexation and unpackaging of fluorescent siRNA was monitored via FRET.[15] FRET-based photoisomerization of azobenzene nanovalves has been used as a mechanism to trigger release of camptothecin from mesoporous silica nanoparticles.[16] However, studies have revealed some limitations with organic dyes for examining FRET, such as emission spectral overlap and photobleaching.[13] Consequently, FRET systems that can prevent these issues have been examined including inorganic quantum dots[12] or luminescent lanthanides,[5,8] which offer higher stability from photobleaching, large Stokes shifts between excitation and emission bands, and long luminescence lifetimes to minimize spectral overlap.

A variety of vehicles have been developed to encapsulate siRNA into nanoparticles to enhance stability and cellular internalization.[17,18] For example, we have previously developed two trehalose-based polymeric systems, one via a copper (I) catalyzed click reaction[19] (yielding an alternating structure) and another via RAFT polymerization that yielded a diblock polymer coated with poly(trehalose).[20] The block copolycation was demonstrated to promote colloidal stability, lyoprotection, and effective siRNA delivery.[20] It has also been reported by Tseng et. al. that the presence of trehalose can increase delivery efficiency for PEI-pDNA polyplex systems.[21]

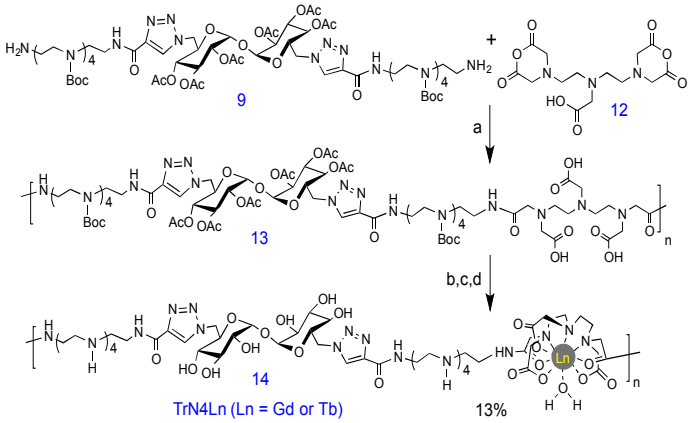

Scheme 1. Monomer polymerization, amine deprotection and lanthanide chelation (note that all steps were performed at room temperature, r.t.).

[†] *University of Minnesota Department of Chemistry, 207 Pleasant Street SE, Minneapolis, MN 55455*
§Virginia Tech Department of Chemistry and Macromolecules and Interfaces Institute, 900 West Campus Drive, Blacksburg, VA 24061-0001
[‡]Wake Forest Institute for Regenerative Medicine and Virginia Tech-Wake Forest School of Biomedical Engineering and Sciences, Winston-Salem, NC 27101
*To whom correspondence should be addressed: treineke@umn.edu

Herein, we describe a new trehalose-based polycation that contains lanthanide chelates for siRNA delivery and monitoring. The trehalose moieties serve to enhance cellular delivery and promote stability, the lanthanide domains provide imaging capability (luminescence and magnetic resonance), and the oligoethyleneamine domains promote electrostatic interaction and polyplex formation with siRNA. Furthermore, this system was developed as a tool to monitor polyplex packaging *in vitro* by including LRET (lanthanide resonance energy transfer) pairs in the design, i.e., a Tb^{3+}-chelated polymer donor with a tetramethyl rhodamine (TMR)-labeled siRNA acceptor.

To create the target materials, hexa-O-acetyl-diazido-D-trehalose (Scheme S1) and a terminal alkyne-functionalized protected oligoethyleneamine (Scheme S2) were first synthesized according to our previously published procedures.[22] The macromonomer was then created via copper (I) catalyzed azide-alkyne cycloaddition followed by deprotection of the Cbz groups. The diamine macromonomer (TrN4) was copolymerized with DTPA-BA (Scheme 1) to yield the polymer precursor. The polymers were deprotected and chelated with lanthanide ions to yield the final polymer TrN4Ln.

The polymers chelated with Gd^{3+} and Tb^{3+} were purified by exhaustive dialysis (to remove free metals), then lyophilized, and analyzed via gel permeation chromatography, static light scattering, and inductively coupled plasma optical emission spectroscopy (ICP-OES)(Supporting Information). The M_w was found to be 13.0 kDa corresponding to a degree of polymerization (n_w) equal to 10. The ICP-OES data revealed the lanthanide content and theGd^{3+} and Tb^{3+} mass content were found to be 8.65% and 8.62%, respectively. Based on the theoretical lanthanide mass percentages (11.9% and 12.0%, respectively), about 72% of the DTPA chelates contain lanthanides. The luminescent lifetime (τ) of the Tb^{3+} chelated polymer (TrN4Tb) was examined in both D_2O (τ = 1.62 msec) and H_2O (τ = 1.27 msec). The revised Horrocks equation was applied to calculate the number of water coordination sites (q) per chelate unit, which was 0.25,[23] a value lower than expected for this polymer system. Previously, our group has published similar polycation chelate structures that lack trehalose (N4Gd and N4Tb) and found that applying the revised Horrock's equation to luminescence lifetime measurements in the presence of D_2O and H_2O revealed q values of 0.7-0.8 [i.e., D_2O (τ = 2.8 msec) and H_2O (τ = 1.6 msec)].[8] Thus, we believe that the presence of trehalose, which contains significant –OH oscillators in the second coordination sphere, could promote some direct metal chelation and/or further nonradiative relaxation pathways of the chelate structures in D_2O (via –OH oscillation on the trehalose). This effect could play a role in the lower calculated q value than the expected value near 1.

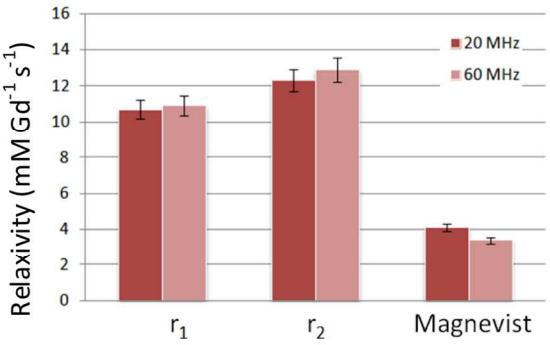

Figure 1. Relaxivity measurements for TrN4Gd and Magnevist according to water relaxation rate constants at 0.47 Tesla (20 MHz) and 1.4 Tesla (60 MHz) at 37 °C.

Figure 1 summarizes the effect of TrN4Gd on both the T_1 and T_2 relaxivity (r_1 and r_2, respectively) of water protons at magnetic fields of 0.47 T and 1.41 T (20 and 60 MHz, respectively) at 37 °C in dilute aqueous solutions. The r_1 values at both 0.47 T and 1.4 T were found to be 10.7 and 10.9 $mM^{-1}s^{-1}$, respectively and the r_2 values were 12.3 and 12.9 $mM^{-1}s^{-1}$, respectively. Compared to the commercially-available MRI contrast agent Magnevist, TrN4Gd achieved more than double the relaxivity per Gd^{3+} ion. These relaxivity values are in line with similar polymers lacking trehalose (N4Gd).[5,8] It should be noted that we have previously shown that relaxivity values of the free polymer (that contains Gd^{3+} chelates, N4Gd, Figure S2) are very similar to polyplexes formed with the same chelated polymer.[5,8]

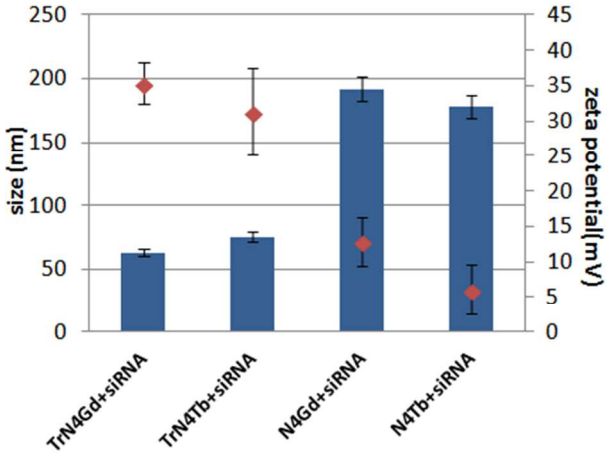

Figure 2. Dynamic light scattering and Zeta potential of polyplexes at N/P = 40. The blue bar graph represents the particle radius and the red diamonds indicate the Zeta potential values of polyplex formulations in water. The error bars represent the standard deviation for three measurements.

To understand the role of trehalose in polyplex formation, two control polymers previously published by our group, N4Gd and N4Tb, that lacked trehalose (Figure S2) with M_w of 16.0 kDa (n_w = 25) were also examined and compared to the TrN4 systems for their ability to form polyplexes.[8] Because each repeat unit within the trehalose polymer has two pentaethyleneamine domains (20 in total, n_w = 10), the total number of pentaethyleneamine units (25) within the N4Gd and N4Tb polymers

are comparable to that present in the trehalose-containing polymers. However, it should be noted that the number of lanthanide chelate domains are half as abundant in the trehalose system. Gel electrophoresis shift assays (Figure S3) indicate that the trehalose-containing polymers (TrN4Gd and TrN4Tb) bind and complex siRNA into polyplexes at a polymer amine (N) to RNA phosphate (P) ratio (N/P ratio) of 10 (as indicated by the lack of migration in the electrophoretic field). However, the polycations lacking trehalose (N4Gd and N4Tb) do not fully complex siRNA as indicated by siRNA migration at all N/P ratios. Figure 2 presents dynamic light scattering (DLS) and Zeta potential results showing that polymers TrN4Gd (R_h = 63 nm, ζ = 35 mV) and TrN4Tb (R_h = 75 nm, ζ = 31 mV) formed much smaller/tighter polyplexes and had more positive Zeta potentials compared to N4Gd (R_h = 190 nm, ζ = 13 mV) and N4Tb (Rh = 180 nm, ζ = 6.1 mV). These results indicate that trehalose plays a role in more strongly binding siRNA, likely through hydrogen bonding of the hydroxyls to the nucleic acid backbone, and thus offers favorable properties for cellular siRNA delivery.

As an initial proof of concept experiment to monitor polymer-siRNA association, we examined LRET (Figure 3) between Tb^{3+} on the polymer backbone (donor) and TMR-labeled siRNA (acceptor). Upon polyplex formation, the donor and acceptor are closer (within 10-100 Å distance, allowing LRET). LRET can be monitored in two ways, either via an increase in emission of the acceptor TMR (due to binding and energy transfer from the donor) or via a decrease in the donor (Tb^{3+}) luminescence, indicating lanthanide energy transfer to the TMR-siRNA acceptor in the polyplexes. Herein, the latter case was monitored (the decrease in Tb^{3+} emission) due to interference with direct excitation of TMR at 345 nm (explained below). The luminescence donor, Tb^{3+}, can be excited at 345 nm and yields emission peaks at 495, 550, 588, and 620 nm (as shown in Figure 3a-c, green, blue, and purple lines). TMR has a broad and intense excitation band centered around 530 nm, which overlaps with the two primary emission bands of Tb^{3+} (495 and 550 nm). It should be noted that TMR also has weak absorbance bands at λ_{ex} = 245 nm, 278 nm, and 345 nm (which is why TMR-siRNA shows emission in Figure 3 as it is also directly excited at 345 nm). However, LRET can still be observed in this system by monitoring a decrease in Tb^{3+} emission at 495 and 550 nm. The broad TMR emission peak is found at 595 nm as shown in Figure 3 (red lines) but can be time gaited out (*vide infra*).

In an attempt to monitor polyplex formation via LRET, four solutions containing TrN4Tb polymer only, TMR-siRNA only, TrN4Tb/TMR-siRNA polyplexes at N/P = 40, and TrN4Tb/siRNA (no TMR) polyplexes at N/P = 40 were formulated, excited at 345 nm, and monitored by collecting the emission spectra after three different delay times (20, 40, and 50 µsec). It should be noted that the emission spectra were collected after different delay times to clarify monitoring of Tb^{3+}-TMR LRET upon polyplex formation via a decrease in Tb^{3+} emission. The interfering TMR fluorescence, which is short-lived compared to the very long lifetime Tb^{3+} luminescence emission (ms time scale), can be gated out of the spectra by optimizing the delay time. Upon excitation at 345 nm, Tb^{3+} energy transfer was promoted and observed in all three spectra as a decrease in the TrN4Tb/TMR-siRNA polyplex emission intensity (see 495 and 550 nm peaks, green spectra lines) as compared to the emission intensity of the TrN4Tb polymer only and TrN4Tb-siRNA controls lacking TMR (see 495 and 550 nm peaks, blue and purple spectra lines). This indicated polyplex formation through the decrease in Tb^{3+} emission due to energy transfer to TMR.

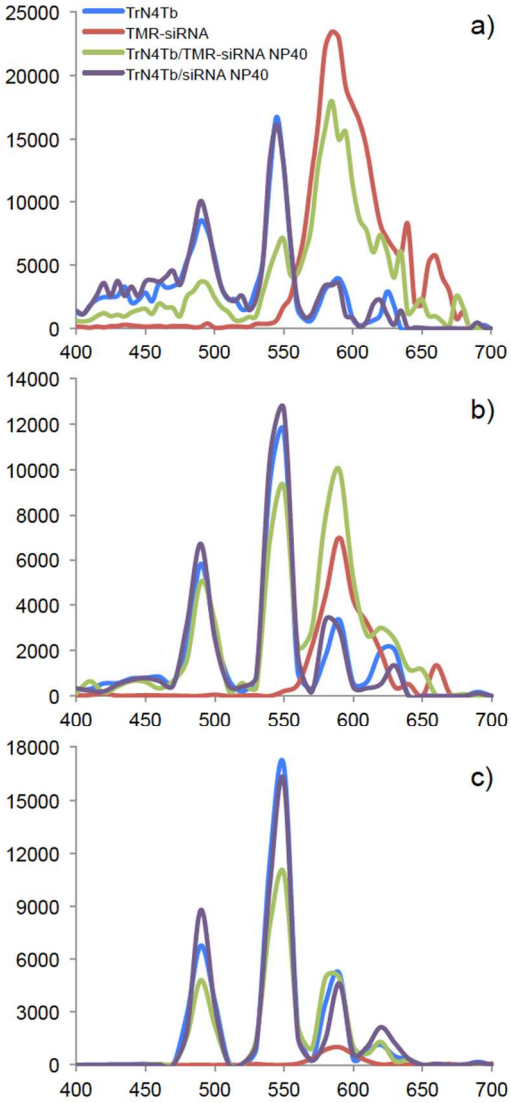

Figure 3. LRET study of TrN4Tb/TMR-siRNA complexation (green lines). TrN4Tb polymer only (blue lines), TMR-siRNA only (red lines), and polyplexes formulated with TrN4Tb-siRNA without TMR (purple lines) were also examined as controls. All polyplex formulations were created at N/P = 40 (polymer only and siRNA only were diluted at equivalent concentrations) and the emission spectra collected at 345 nm. a) Emission spectra of the formulations collected after a delay time of 20 µsec. b) Emission spectra collected after a delay time of 40 µsec. c) Emission spectra collected after a delay time of 50 µsec. Decrease in intensity of the key TrN4Tb/TMR-siRNA signals (green, 495 and 550 nm peaks) in all three spectra due to LRET confirms polyplex formation.

Increasing the delay time to gait out interfering TMR fluorescence was used to further clarify the decrease in Tb^{3+} emission. TMR fluorescence is clearly evident in the TMR-siRNA and polyplex spectra collected after a 20 µsec delay time, and the TMR clearly overlaps with the Tb^{3+} luminescence spectrum (see broad emission peak 550 nm – 680 nm, red and green lines). However, as we increased the delay time to 40 and 50 µsec (Figure 3b and 3c), the short-lived TMR fluorescence was

increasingly gated out of the emission spectrum (notice the decrease in the broad emission peak 550 nm – 680 nm, red and green lines). At a 50 µsec delay time (Figure 3c), the TMR peak was virtually absent (only a very small emission peak for TMR-siRNA was observed in the TMR-siRNA only control, red line). Using this optimized delay, our key observation is that the Tb^{3+} donor emission peaks at 495 and 550 nm (green lines) decreased upon polyplex formation due to polymer-siRNA binding and LRET of Tb^{3+} emission to TMR-siRNA as compared to the controls of TrN4Tb (blue lines) and TrN4Tb/siRNA (no TMR) polyplexes. Also, we note that the longer wavelength emission lines of Tb^{3+} (588 and 620 nm) did not decrease in intensity (no LRET to TMR from these emission bands). These results indicate that stable polyplexes were formed with this polymer, and this vehicle design motif offers the ability to monitor siRNA packaging (and possibly unpackaging) by monitoring LRET in a time-gated manner.

a)

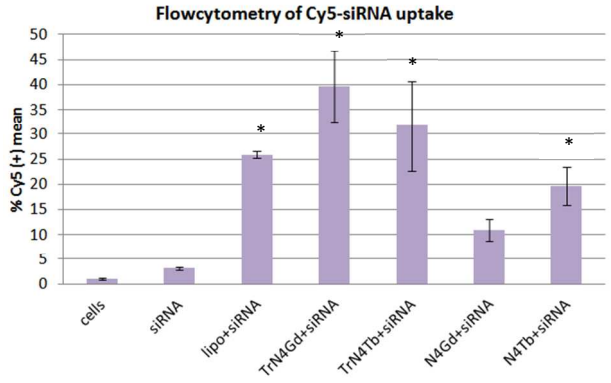

b)

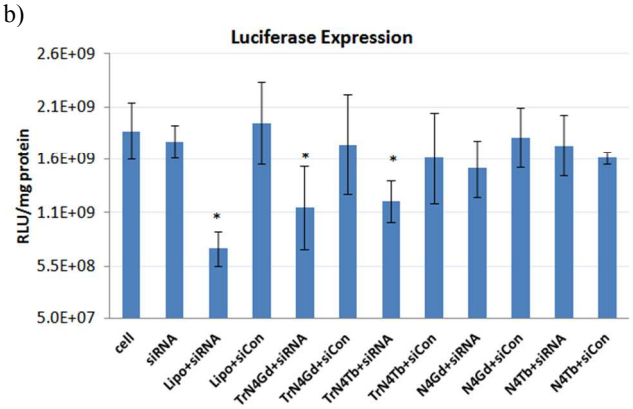

Figure 4. Cellular delivery of siRNA with the polyplex formulations (TrN4Gd, TrN4Tb, N4Gd, and N4Tb) and controls (cells only, siRNA only, and Lipofectamine-siRNA). Polyplexes were formed at an N/P ratio of 40 and Lipofectamine complexes were formulated at the manufacturers recommended conditions. All experiments were performed in triplicate and error bars represent standard deviations. (a) Cellular internalization of siRNA. The percentage of Cy5-siRNA-positive cells 4 h after transfection was determined using flow cytometry analysis. Values found to be statistically different from the cells-only control are marked with an * (according to a student's t-test with $p < 0.05$). (b) siRNA-mediated luciferase gene knockdown in luciferase-expressing human glioblastoma (U87) cells. Gene knockdown found to be statistically different from the siCon control (for the same delivery vehicle) are marked with an * (according to a student's t-test with $p < 0.05$).

The polyplex formulations were further examined in cultured cells for internalization and gene knockdown efficacy with cultured glioblastoma cells (U87) that stably express luciferase (Figure 4). Prior to flow cytometry analysis, cell surface bound polyplexes were removed through trypinization, CellScrub™ and multiple phosphate buffered saline washes (see Supporting Information). The trehalose-containing lanthanide polymers, TrN4Gd and TrN4Tb, revealed a higher cellular uptake of Cy5-labeled siRNA (30-40% of cells positive for siRNA, Figure 4a) than that observed with Lipofectamine (25% of cells positive for siRNA). Interestingly, the polyplexes formed with analogous polymers lacking trehalose (N4Tb and N4Gd), showed very low siRNA internalization (10-20% cells positive for siRNA) and the results from the N4Gd-siRNA formulation was not statistically different from the cells only control. As shown in Figure 4b, the trehalose polyplex formulations also revealed the highest luciferase gene knockdown (40% and 37%, luciferase down regulation, respectively) when compared to the N4Gd and N4Tb polyplexes. Strikingly, the polyplex formulations lacking trehalose did not show any measurable siRNA-mediated gene knockdown (not statistically different than the negative controls). Lastly, MTT assay results revealed minimal cytotoxicity of all these polyplex formulations in U87 cells at N/P ratio of 40 (Supporting Information).

In summary, we have successfully synthesized a polymer that offers a lanthanide chelate copolymerized with trehalose and cationic domains for the encapsulation, delivery, and monitoring of siRNA delivery. Numerous properties of the polymer were examined such as complexation with siRNA, polyplex size, NMR relaxivity, and LRET-based monitoring of polyplex formation. The flow cytometry and luciferase gene knockdown experiments were conducted with U87 cells, revealing that delivery efficiency and siRNA-mediated gene knockdown was significantly improved upon incorporating trehalose domains into the polymeric backbone. Indeed, lanthanide-containing polymeric delivery vehicles offer a design model to build theranostic systems for the *in situ* monitoring of nucleic acid packaging, decomplexation, and delivery through monitoring LRET. Future studies will include further synthetic optimization of these systems for improving gene knockdown such as examining the role of polymer molecular weight,[19,24] increasing the length of the oligoethyleneamine block,[24,25] and promoting polymer degradation.[26] In addition, future studies are also aimed at monitoring delivery and nucleic acid unpackaging within cells in a time-gated manner and understanding chelate stability in biological conditions.

ACKNOWLEDGEMENT

This project was funded by the National Science Foundation (DMR 1105895). We acknowledge Dr. Karina Kizjakina for helpful discussions and Dr. Nilesh Ingle for the statistical analysis in Figure 4.

REFERENCES

(1) Chen, G.; Qiu, H.; Prasad, P. N.; Chen, X. *Chem. Rev.* **2014**, *114,* 5161.
(2) Fan, Z.; Senapati, D.; Singh, A. K.; Ray, P. C. *Mol. Pharm.* **2013**, *10*, 857.
(3) Santra, S.; Perez, J. M. *Biomacromolecules* **2011**, *12*, 3917.
(4) Guo, Y.; Chen, W.; Wang, W.; Shen, J.; Guo, R.; Gong, F.; Lin, S.; Cheng, D.; Chen, G.; Shuai, X. *ACS Nano* **2012**, *6*, 10646.

(5) Bryson, J. M.; Fichter, K. M.; Chu, W.-J.; Lee, J.-H.; Li, J.; Madsen, L. A.; McLendon, P. M.; Reineke, T. M. *Proc. Natl. Acad. Sci. U.S.A.* **2009**, *106*, 16913.
(6) Wang, X.; Chen, Y.; Xue, L.; Pothayee, N.; Zhang, R.; Riffle, J. S.; Reineke, T. M.; Madsen, L. A. *J. Phys. Chem. Lett.* **2014**, *5*, 3825.
(7) Jokerst, J. V.; Gambhir, S. S. *Acc. Chem. Res.* **2011**, *44*, 1050.
(8) Kelkar, S. S.; Xue, L.; Turner, S. R.; Reineke, T. M. *Biomacromolecules* **2014**, *15*, 1612.
(9) Kelkar, S.; Reineke, T. M. *Bioconjugate Chem.*, **2011**, *22*, 1879.
(10) Jiang, R.; Lu, X.; Yang, M.; Deng, W.; Fan, Q.; Huang, W. *Biomacromolecules* **2013**, *14*, 3643.
(11) Schneider, S.; Lenz, D.; Holzer, M.; Palme, K.; Süss, R. *J. Controlled Release* **2010**, *145*, 289.
(12) Kim, H.; Ng, C. Y. W.; Algar, W. R. *Langmuir* **2014**, *30*, 5676.
(13) Domingo, B.; Sabariegos, R.; Picazo, F.; Llopis, J. *Microsc. Res. Tech.***2007**, *70*, 1010.
(14) Bryson, J.; Chu, W. ‐ J.; Lee, J. ‐ H.; Reineke, T. M. *Bioconjugate Chem.* **2008**, *19*, 1505.
(15) Endres, T.; Zheng, M.; Kılıç, A.; Turowska, A.; Beck-Broichsitter, M.; Renz, H.; Merkel, O. M.; Kissel, T. *Mol. Pharm.* **2014**, *11*, 1273.
(16) Croissant, J.; Chaix, A.; Mongin, O.; Wang, M.; Clément, S.; Raehm, L.; Durand, J.-O.; Hugues, V.; Blanchard-Desce, M.; Maynadier, M.; Gallud, A.; Gary-Bobo, M.; Garcia, M.; Lu, J.; Tamanoi, F.; Ferris, D. P.; Tarn, D.; Zink, J. I. *Small* **2014**, *10*, 1752.
(17) Tseng, Y. C.; Mozumdar, S.; Huang, L. *Adv. Drug Deliv. Rev.* **2009**, *61*, 721.
(18) Oishi, M.; Nagasaki, Y.; Itaka, K.; Nishiyama, N.; Kataoka, K. *J. Am. Chem. Soc.* **2005**, *127*, 1624.
(19) Xue, L.; Ingle, N. P.; Reineke, T. M. *Biomacromolecules* **2013**, *14*, 3903.
(20) Sizovs, A.; Xue, L.; Tolstyka, Z. P.; Ingle, N. P.; Wu, Y.; Cortez, M.; Reineke, T. M. *J. Am. Chem. Soc.* **2013**, *135*, 15417.
(21) Tseng, W.-C.; Tang, C.-H.; Fang, T.-Y.; Su, L.-Y. *Biotechnol. Prog.* **2007**, *23*, 1297.
(22) Srinivasachari, S.; Liu, Y.; Zhang, G.; Prevette, L.; Reineke, T. M. *J. Am. Chem. Soc.* **2006**, *128*, 8176.
(23) Beeby, A.; Clarkson, I.M.; Dickins, R.S.; Faulkner, S.; Parker, D.; Royle, L.; de Sousa, A.S.; Williams, J.A.G.; Woods, M. *J. Chem. Soc., Perkin Trans. 2* **1999**, 493.
(24) Kizjakina, K.; Bryson, J. M.; Grandinetti, G.; Reineke, T. M. *Biomaterials* **2012**, 33, 1851.
(25) Smith, A. E.; Sizovs, A.; Grandinetti, G.; Xue, L.; Reineke, T. M. *Biomacromolecules* **2011**, 12 , 3015.
(26) Liu, Y.; Reineke, T. M. *Biomacromolecules* **2010**, 316.

TOC graphic: